Buoyancy-driven convection with a uniform magnetic field. Part 1. Asymptotic analysis

By T. ALBOUSSIÈRE[1], J. P. GARANDET[1] AND R. MOREAU[2]

[1] Commissariat à l'Energie Atomique DTA/CEREM/DEM/SESC, Centre d'Etudes Nucléaires de Grenoble, 85 X, 38041 Grenoble Cedex, France

[2] INPG Laboratoire Madylam UA CNRS 1326, ENSHMG, BP 95, 38402 St Martin d'Hères Cedex, France

We study the convection of an electrically conducting liquid in a horizontal cylinder (horizontal Bridgman configuration). A uniform steady vertical magnetic field is externally imposed. The thermal and magnetic Prandtl numbers are assumed equal to zero. The thermal field is obtained assuming pure conduction and certain conditions at the boundaries, so that the heat flux is axial and uniform. The influence of the cylinder's cross-sectional shape is examined. In the high Hartmann number limit ($Ha \gg 1$), an analytical solution is found for the fully established flow. With electrically insulating walls, the magnetically damped convective velocity varies as Ha^{-2} when the cross-section has a horizontal plane of symmetry, while it varies as Ha^{-1} for non-symmetrical shapes. When the walls are perfectly conducting, the damped velocity always varies as Ha^{-2}.

1. Introduction

Liquid motions are of crucial importance in crystal growth from a melt: they convect chemical species and control the final solute distribution in the resulting solid. Periodic or random motions, when they develop, are responsible for defects such as the well-known striations (Langlois 1985). Even a steady hydrodynamical regime may produce both lateral and longitudinal macrosegregations, depending on the flow intensity and on the growth conditions (Burton, Prim & Slichter 1953).

Two methods exist in order to reduce these convection effects. First, a reduction of the buoyancy force by a factor of 10^5 may be expected in a microgravity environment (accessible for instance in the NASA space shuttle); this method works for any material. The alternative method is electromagnetic damping, which is only effective for electrically conducting liquids. A steady magnetic field reduces the turbulence level through the Joule effect and also exerts a braking Lorentz force on steady flows (see for instance Moreau 1990).

Pressure-driven flows in ducts with a steady, uniform magnetic field have received great attention. Asymptotic analyses in the high Hartmann number (Ha) range were carried out by Shercliff (1953, 1956), Hunt (1965), Hunt & Stewartson (1965), Hunt & Malcom (1968) and Kulikovskii (1968), and reviewed by Hunt & Shercliff (1971). Different regions (cores and thin boundary layers) can be identified. In the cores, shear stresses are assumed to be negligible compared to Lorentz forces. Hartmann layers of characteristic thickness $Ha^{-1}H$ (H is a typical lengthscale of the cavity) develop along the walls which are not parallel to the magnetic field; such layers strongly interact with the cores. Shear layers of thickness $Ha^{-\frac{1}{2}}H$ develop along surfaces composed of

magnetic field lines. They exist between two cores or near walls parallel to the magnetic field; they are often passive layers but their study is more difficult and may lead to unexpected results such as large velocities.

Buoyancy-driven convection with a magnetic field has received comparatively less attention, except for the Rayleigh–Bénard configuration with a vertical magnetic field (Chandrasekhar 1961). In this particular case, gravity, the magnetic field, the normal to the walls and the temperature gradient are all parallel. Convection in the Czochralski process with an applied magnetic field has also been studied (Langlois 1985), theoretically (Hjellming & Walker 1986), numerically (Hjellming 1990) and experimentally (Carlson & Witt 1992). But much rarer are the results concerning the Bridgman method with an applied magnetic field. Analytical exact solutions have been obtained (Gershuni & Zhukhovitskii 1972 and Garandet, Alboussière & Moreau 1992) for idealized configurations where the fluid flow is parallel and one-dimensional (the cross-section shape is not taken into account). Some numerical studies exist (Motakef 1990), but the range of Hartmann numbers considered is unfortunately not very large. Some experimental studies have demonstrated the influence of a magnetic field through measurements of the segregation in the solid (Matthiesen *et al.* 1987) but no velocity measurements have been performed so far.

In this paper, we study the buoyancy-driven convection in a Bridgman type configuration in the presence of a uniform magnetic field from an analytical viewpoint (in the high Hartmann number range, a case often met in practice). We concentrate on the particular influence of the shape of the cavity.

In §2, we consider the MHD governing equations using the new variables, $M^+ = \nabla \times U + Ha J$ and $M^- = \nabla \times U - Ha J$ (where U and J denote the non-dimensional velocity and electric current density fields). These variables are the curls of Elsasser's variables (Elsasser 1950) and similarly facilitate finding the forms of the solutions in the cores and in the boundary layers. Moreover, our variables are more general since the flow need not be parallel and the pressure gradient need not be known *a priori*. With these new variables, flows other than pressure-driven duct flows may be considered, and any geometry and any driving force may be tackled. The key result is the knowledge of the variations of the solutions along any magnetic field line, including through the Hartmann layers. The solution is determined assuming two-dimensional unknown variables for which two-dimensional partial differential equations are derived. Nevertheless, we did not obtain the boundary conditions for these two-dimensional variables in the most general case; such a result would require the local study of the parallel layers.

Section 3 is devoted to an application of the general formulation (§2) to the case of a buoyancy-driven fully established flow in a horizontal cylinder. We assume a vertical magnetic field and a uniform axial thermal gradient. The shape of the cross-section is given through the functions $Z_1(Y)$ and $Z_2(Y)$ describing its upper and lower contours. In this particular case, the above-mentioned boundary conditions for the two-dimensional variables are easily found. According to our results, the flow greatly depends on the precise shape of the cavity and on the electric conditions at the walls.

2. Asymptotic analytical model ($Ha \gg 1$)

Let us consider an electrically conducting fluid in a cavity of typical lengthscale H with a steady, uniform magnetic field B. We also assume that:

(i) the magnetic Reynolds number $R_m = \mu \sigma U H$ is very small compared to unity

(U stands for the velocity scale and μ, σ for magnetic permeability and electric conductivity), so that the magnetic field is not perturbed by the velocity field;

   (ii) the Hartmann number $Ha = (\sigma/\rho v)^{\frac{1}{2}} BH$ is large compared to unity, so that viscous stresses are negligible in the main part of the cavity. Here ρ and v are the density and kinematic viscosity;

   (iii) inertia is negligible;

   (iv) body forces, other than electromagnetic ones, are known in the whole cavity, steady and independent of the velocity field;

   (v) the fluid flow is steady: $\partial/\partial t = 0$;

   (vi) the physical properties of the fluid are uniform.

2.1. *Governing equations*

With our assumptions, four basic equations govern the flow, expressing mass conservation (1), electric charge conservation (2), momentum transport (3) and Ohm's law (4):

$$\nabla \cdot u = 0, \tag{1}$$

$$\nabla \cdot j = 0, \tag{2}$$

$$-\nabla p + \rho f + j \wedge B + \rho v \, \Delta u = 0, \tag{3}$$

$$j = \sigma(-\nabla \phi + u \wedge B), \tag{4}$$

where f denotes the non-electromagnetic force field per unit mass and u, j, p, ϕ denote the velocity, the electric current density, the pressure and the electric potential fields. We can eliminate p and ϕ from our problem by taking the curl of (3) and (4):

$$\rho c + (B \cdot \nabla) j + \rho v \, \Delta(\nabla \times u) = 0, \tag{5}$$

$$\nabla \times j = \sigma(B \cdot \nabla) u, \tag{6}$$

where $c = \nabla \times f$. Equations (1), (2), (5) and (6) govern the variables u and j, whereas, in a second step, the variables p and ϕ can be determined using the divergence of (3) and (4) once u and j have been found.

Let us now proceed to make the problem non-dimensional, using the scales

$$X = \frac{x}{H}, \quad U = \frac{uH}{v}, \quad e_b = \frac{B}{B}, \quad J = \frac{jH}{v\sigma B}, \quad C = \frac{cH^4}{v^2}, \quad \Phi = \frac{\phi}{vB}.$$

The system of equations (1), (2), (5) and (6) can now be written:

$$\nabla \cdot U = 0, \tag{7}$$

$$\nabla \cdot J = 0, \tag{8}$$

$$C + Ha^2(e_b \cdot \nabla) J + \Delta(\nabla \times U) = 0, \tag{9}$$

$$\nabla \times J = (e_b \cdot \nabla) U. \tag{10}$$

We also use the non-dimensional form of Ohm's law with the electric potential:

$$J = -\nabla \Phi + U \wedge e_b. \tag{11}$$

It appears useful to define the new variables M^+ and M^-:

$$M^+ = \nabla \times U + Ha J, \tag{12}$$

$$M^- = \nabla \times U - Ha J. \tag{13}$$

The curl of (10) gives

$$(e_b \cdot \nabla) \nabla \times U + \Delta J = 0. \tag{14}$$

Considering the combinations $(9) + Ha \times (14)$ and $(9) - Ha \times (14)$, we obtain

$$Ha(e_b \cdot \nabla) M^+ + \Delta M^+ = -C, \tag{15}$$

$$-Ha(e_b \cdot \nabla) M^- + \Delta M^- = -C. \tag{16}$$

The new system of equations (7), (8), (10), (12), (13), (15), (16) is equivalent to the previous one, composed of (7)–(10), but (15) and (16) are very interesting since they involve separately the variables M^+ an M^- and since they express the most important features of MHD. So this new system lends itself better to the derivation of solutions.

Using the definitions of M^+ and M^- (12) and (13), and the continuity equations (7), (8), useful equations are derived:

$$J = (M^+ - M^-)/2Ha, \tag{17}$$

$$\nabla \times U = \tfrac{1}{2}(M^+ + M^-), \tag{18}$$

$$\nabla \cdot M^+ = 0, \tag{19}$$

$$\nabla \cdot M^- = 0. \tag{20}$$

2.2. *The core solution*

A core is a region where the characteristic lengthscale of the variations of the solutions is unity in non-dimensional terms. Since $Ha \gg 1$, we can estimate *a priori* the Laplacian terms in (15) and (16), and then rewrite these equations for a core:

$$(e_b \cdot \nabla) M^+ = -\frac{C}{Ha}\left[1 + O\left(\frac{1}{Ha}\right)\right], \tag{21}$$

$$(e_b \cdot \nabla) M^- = \frac{C}{Ha}\left[1 + O\left(\frac{1}{Ha}\right)\right], \tag{22}$$

where the terms $O(1/Ha)$ stand for the neglected Laplacian terms. For a given core region, the core solutions M_c^+ and M_c^- are the solutions of (15) and (16), also satisfying (21) and (22), that identify with the actual solutions in this core. These solutions are defined in the whole fluid domain and take the form

$$M_c^+ = -\frac{1}{Ha}\int_0^Z C(X, Y, Z')\,\mathrm{d}Z'\left[1 + O\left(\frac{1}{Ha}\right)\right] + M_2^+(X, Y), \tag{23}$$

$$M_c^- = \frac{1}{Ha}\int_0^Z C(X, Y, Z')\,\mathrm{d}Z'\left[1 + O\left(\frac{1}{Ha}\right)\right] + M_2^-(X, Y). \tag{24}$$

Here, Z denotes the spatial coordinate in the magnetic field direction and X, Y denote the spatial coordinates in the orthogonal plane, such that the vectors e_x, e_y, e_z define a direct orthonormal frame of reference ($e_b = e_z$). The unknown vector fields $M_2^+(X, Y)$ and $M_2^-(X, Y)$ appear when integrating (21) and (22) and vary over $O(1)$ lengthscales (the subscript 2 indicates that these fields are two-dimensional since they are independent of Z).

2.3. *The boundary layers*

A boundary layer is a region where the characteristic lengthscale of the variations of the solutions is very small compared to unity. The difference between the actual solutions and the core solutions is obtained by subtracting (15) and (16) applied to the core solutions from (15) and (16) applied to the actual solutions:

$$Ha(e_b \cdot \nabla)[M^+ - M_c^+] + \Delta[M^+ - M_c^+] = 0, \tag{25}$$

$$-Ha(e_b \cdot \nabla)[M^- - M_c^-] + \Delta[M^- - M_c^-] = 0. \tag{26}$$

In these boundary layers (19) and (20) take the form

$$\nabla \cdot [M^+ - M_c^+] = 0, \tag{27}$$

$$\nabla \cdot [M^- - M_c^-] = 0. \tag{28}$$

In the following, n denotes a unit vector normal to the layer (direction of greatest variations), while n denotes the associated spatial coordinate and δ denotes the characteristic thickness of the layer. When n is orthogonal to e_b, and the variations in the n-direction are assumed to be dominant ($\partial/\partial n = O(1/\delta)$), equations (25) and (26) become

$$Ha\frac{\partial}{\partial Z}[M^+ - M_c^+] + \left\{\frac{\partial^2}{\partial n^2}[M^+ - M_c^+]\right\}[1 + O(\delta^2)] = 0, \tag{29}$$

$$-Ha\frac{\partial}{\partial Z}[M^- - M_c^-] + \left\{\frac{\partial^2}{\partial n^2}[M^- - M_c^-]\right\}[1 + O(\delta^2)] = 0. \tag{30}$$

Since $\partial/\partial Z = O(1)$ (in the magnetic field direction the characteristic lengthscale is unity), one can estimate the characteristic thickness of this so-called parallel layer: $\delta = O(Ha^{-\frac{1}{2}})$. Such a parallel layer develops in the vicinity of a wall parallel to the magnetic field or between two cores which cannot be matched with the core solutions (23) and (24).

A boundary layer where $\cos(e_b, n)$ is not zero is called a Hartmann layer, where (25) and (26) can be rewritten

$$Ha\cos(e_b, n)\left\{\frac{\partial}{\partial n}[M^+ - M_c^+]\right\}[1 + O(\delta)] + \left\{\frac{\partial^2}{\partial n^2}[M^+ - M_c^+]\right\}[1 + O(\delta^2)] = 0, \tag{31}$$

$$-Ha\cos(e_b, n)\left\{\frac{\partial}{\partial n}[M^- - M_c^-]\right\}[1 + O(\delta)] + \left\{\frac{\partial^2}{\partial n^2}[M^- - M_c^-]\right\}[1 + O(\delta^2)] = 0. \tag{32}$$

The characteristic thickness is clearly $\delta = O(Ha^{-1})$. In the following, we call θ the vector angle between n and e_b (with n directed into the fluid), S^+ a surface where $\cos\theta > 0$ and S^- a surface where $\cos\theta < 0$. Using the continuity equations (27) and (28), equations (31) and (32) lead to analytical expressions for the solutions in the Hartmann layers (see derivation in the Appendix):

Projection on the tangent plane of the layer (subscript t):

$$(M^+ - M_c^+)_t = \left[1 + O\left(\frac{1}{Ha}\right)\right]M_0^+ e^{-Ha|\cos\theta|n}, \tag{33}$$

$$(M^- - M_c^-)_t = \left[1 + O\left(\frac{1}{Ha}\right)\right]M_0^- e^{-Ha|\cos\theta|n}, \tag{34}$$

where M_0^+ (resp. M_0^-) is a vector field tangent to the cavity wall, independent of the n-coordinate and exactly zero if $\cos\theta < 0$ (resp. $\cos\theta > 0$). Indeed, M^+ has no Hartmann layer on one side and M^- on the other side.

Normal component:

$$(M^+ - M_c^+)\cdot n = \left[1 + O\left(\frac{1}{Ha}\right)\right]\left[Ha^{-1}\nabla_{s^+}\cdot\left(\frac{M_0^+}{|\cos\theta|}\right) - n\frac{M_0^+\cdot\nabla|\cos\theta|}{|\cos\theta|}\right]e^{-Ha|\cos\theta|n}, \tag{35}$$

$$(M^- - M_c^-)\cdot n = \left[1 + O\left(\frac{1}{Ha}\right)\right]\left[Ha^{-1}\nabla_{s^-}\cdot\left(\frac{M_0^-}{|\cos\theta|}\right) - n\frac{M_0^-\cdot\nabla|\cos\theta|}{|\cos\theta|}\right]e^{-Ha|\cos\theta|n}, \tag{36}$$

where the differential operators $\nabla_{s^+}\cdot$ and $\nabla_{s^-}\cdot$ denote the divergence operators applied to vectors tangent to the surfaces S^+ and S^-.

The precision of this asymptotic analysis ($Ha \gg 1$) appears to be of order Ha^{-1} both in the cores and in the Hartmann layers (see the Appendix); we thus expect a Ha^{-1} precision for our final solution. In the following, we leave aside these considerations of precision; the reader can check that they remain valid.

2.4. *Return to the variables U and J*

Using the variables M^+ and M^-, we were able to find the correct form of the asymptotic solution. We have two reasons to return now to the variables U and J. First, they are physically more interesting in the applications, but more important we cannot complete the calculation of M^+ and M^- because sufficient boundary conditions are not available: so far, we have used (14) which is the curl of Ohm's law but we have not exploited Ohm's law itself (10).

Equation (17) in the core and (23) and (24) give

$$J_c = J_2(X, Y) - Ha^{-2} \int_0^Z C(X, Y, Z') \, dZ', \tag{37}$$

where $J_2 = (M_2^+ - M_2^-)/2Ha$. Ohm's law (10) leads after integration to

$$U_c = U_2(X, Y) + Z \nabla \times J_2(X, Y) - Ha^{-2} \int_0^Z \nabla \times \left\{ \int_0^{Z'} C(X, Y, Z'') \, dZ'' \right\} dZ', \tag{38}$$

where both U_2 and J_2 are independent of the Z coordinate. The equations (7) and (8) in the core imply

$$\nabla \cdot J_2 = Ha^{-2} \nabla \cdot \left\{ \int_0^Z C \, dZ' \right\}, \tag{39}$$

$$\nabla \cdot U_2 = -e_Z \cdot \nabla \times J_2 + Ha^{-2} \nabla \cdot \left\{ \int_0^Z \nabla \times \left\{ \int_0^{Z'} C \, dZ'' \right\} dZ' \right\}. \tag{40}$$

Let us now express the variables U and J in the Hartmann layers. First, using (17) and the solutions (33)–(36) for the Hartmann layers, we obtain

$$(J - J_c)_t = \frac{M_0^+ - M_0^-}{2Ha} e^{-Ha|\cos\theta|n}, \tag{41}$$

where the subscript t denotes the tangential part, and

$$(J - J_c) \cdot n = \left[\frac{Ha^{-2}}{2} \nabla_{s\pm} \cdot \left(\frac{M_0^+ - M_0^-}{|\cos\theta|} \right) - n \frac{(M_0^+ - M_0^-) \cdot \nabla |\cos\theta|}{2Ha|\cos\theta|} \right] e^{-Ha|\cos\theta|n}. \tag{42}$$

Secondly we obtain $U - U_c$ from Ohm's law (10):

$$\nabla \times (J - J_c) = (e_b \cdot \nabla)(U - U_c). \tag{43}$$

Using the curl of (41), we easily deduce the tangential part when integrating between n and infinity:

$$(U - U_c)_t = \frac{Ha^{-1} n \wedge (M_0^+ + M_0^-)}{2|\cos\theta|} e^{-Ha|\cos\theta|n}. \tag{44}$$

And using a method analogous to the one used in the Appendix for M^+ and M^-, the normal component is deduced from the mass conservation equation (7):

$$(U - U_c) \cdot n = \left[\frac{Ha^{-2}}{2} \nabla_{s\pm} \cdot \left(\frac{n \wedge (M_0^+ + M_0^-)}{|\cos\theta|^2} \right) - n \frac{[n \wedge (M_0^+ + M_0^-)] \cdot \nabla |\cos\theta|}{2Ha|\cos\theta|^2} \right] e^{-Ha|\cos\theta|n}. \tag{45}$$

One can check that those expressions for the velocity field are compatible with the expressions obtained for M^+ and M^- in the Hartmann layer.

To sum up this asymptotic analysis, we have obtained the general form of the electric current and velocity fields in the cores, (37) and (38), and in the Hartmann layers, (41), (42) and (44), (45). This form features the two-dimensional variables M_0^+, M_0^-, U_2, J_2 with the following constraints: the boundary conditions for U and J must be satisfied; equations (39) and (40) must be satisfied; M_0^+ and M_0^- must be tangent to S^+ and S^- respectively (remember that they have a zero value on one side, depending on the sign of $\cos\theta$).

These conditions lead to a two-dimensional partial differential system for the four two-dimensional variables. But it is necessary to express the boundary conditions for the two-dimensional domain involved (a projection of the actual three-dimensional geometry in the plane orthogonal to the magnetic field, since the equations are obtained by integration along the magnetic field lines). In the following application, we propose a solution for a case where these boundary conditions can be found.

3. Application to a buoyancy-driven-convection configuration

3.1. *Modelling of the physical problem*

We now focus on buoyancy-driven convection in an idealized horizontal Bridgman furnace. We assume that only thermal buoyancy acts as a driving force and we neglect solutal buoyancy (dilute alloy approximation). Conversely, the induced velocity field can be considered as a fundamental input for the governing equations of the solute distribution. Controlling the flow is hence of the utmost importance. We take into account the influence of B, an externally applied uniform steady vertical magnetic field. The crucible is modelled as a finite-length cylinder with its axis parallel to the e_x direction. Its cross-sectional shape is of typical length H and is defined by its upper and lower contour equations $Z_1(Y)$ and $Z_2(Y)$ in the non-dimensional coordinates (figure 1). The cylinder ends with two plane walls which are a distance L apart; the aspect ratio H/L is supposed to be small enough for a fully established flow to exist in the middle.

We also assume that the thermal Péclet number is very small compared to unity, so that the heat and momentum problems are decoupled. Assuming the two endwalls to be at temperatures T_0 and $T_0 + \Delta T$ respectively and the cylindrical wall to be surrounded by a perfectly thermally insulating medium, the law of heat conduction leads to the solution:

$$T = T_0 + Gx, \tag{46}$$

where $G = \Delta T/L$. The temperature gradient is uniform: $G = G e_x$. Assuming that the Boussinesq approximation holds, the buoyancy force is expressed as $f = [1 - \beta(T - T_0)]g$ ($g = -g e_z$ is the gravity vector). This problem can be handled in the framework of the previous section with $C = -Gr e_Y$, where $Gr = \beta g G H^4/\nu^2$ is the Grashoff number. In our model, the cold wall ($T = T_0$) represents the solidification front, but we assume it is immobile. We only consider the fully established flow ($\partial/\partial X = 0$), far enough from the endwalls. Garandet *et al.* (1992) have shown that, in a two-dimensional Bridgman-like cavity in the (e_X, e_Z)-plane, the end regions have a thickness which varies as $Ha^{-\frac{1}{2}}$ (when $Ha \gg 1$). The solution for the fully established flow is needed in order to calculate the flow near the solidification front which is the most important for solutal segregation.

For boundary conditions, the velocity is zero at the walls, and this study is limited to the two ideal electrical conditions: perfectly insulating (see §3.2) and perfectly conducting walls (see §3.3). Notice that, in each case, it is not necessary to specify the wall thickness.
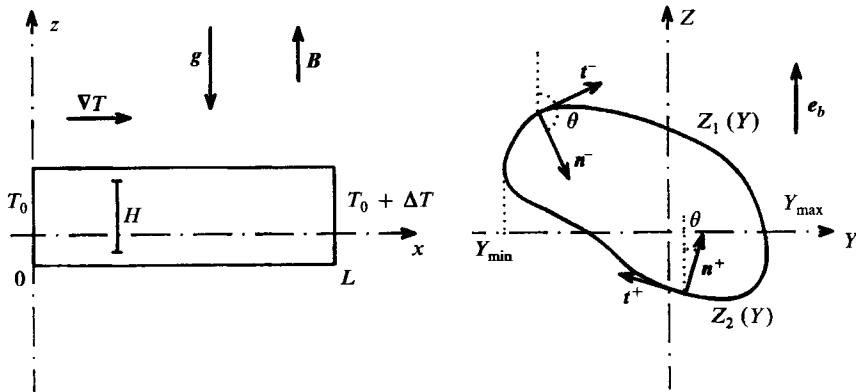
FIGURE 1. The configuration studied.

In the notation of figure 1, Z_1 corresponds to an S^- surface in the previous section, and Z_2 corresponds to S^+. For the following calculations, the coordinate transformation from (e_Y, e_Z) into (n, t) near the walls in the cross-section is useful (figure 1). The vectors n^+ and n^- (resp. t^+ and t^-) denote the normal (resp. tangential) unit vectors to the surfaces S^+ and S^-:

$$n^+(Y) = \frac{-Z_2'}{(1+Z_2'^2)^{\frac{1}{2}}}e_Y + \frac{1}{(1+Z_2'^2)^{\frac{1}{2}}}e_Z, \qquad (47)$$

$$t^+(Y) = \frac{-1}{(1+Z_2'^2)^{\frac{1}{2}}}e_Y - \frac{Z_2'}{(1+Z_2'^2)^{\frac{1}{2}}}e_Z, \qquad (48)$$

$$n^-(Y) = \frac{Z_1'}{(1+Z_1'^2)^{\frac{1}{2}}}e_Y - \frac{1}{(1+Z_1'^2)^{\frac{1}{2}}}e_Z, \qquad (49)$$

$$t^-(Y) = \frac{1}{(1+Z_1'^2)^{\frac{1}{2}}}e_Y + \frac{Z_1'}{(1+Z_1'^2)^{\frac{1}{2}}}e_Z. \qquad (50)$$

The vectors U_2 and J_2 are expressed in the (e_X, e_Y, e_Z) frame of reference, while M_0^+ and M_0^- (which are tangent to S^+ and S^-) are expressed in the (e_X, n, t) frame (see figure 1).

3.2. Perfectly electrically insulating walls

3.2.1. Derivation of the solution

The variables M_0^+, M_0^-, U_2, J_2 are governed by the equations mentioned at the end of the previous section. Their final expressions form the system of (51)–(55) below, where primes denote the $\partial/\partial Y$ derivatives and where some simplifications can be made due to both the condition of fully established flow ($\partial/\partial X = 0$) and the particular form $C = -Gr\,e_Y$:

(i) (51a) and (51b) express that S^+ and S^- are electrically insulating walls ($J \cdot n = 0$). The scalar product $J \cdot n$ comes from (42) with $n = 0$ and $J_c \cdot n$ comes from (37).

(ii) (52a) and (52b) (resp. (52c) and (52d)) express the zero tangential velocity condition along e_X and t on S^+ (resp. on S^-). The tangential part of U is extracted from (44) with $n = 0$ and with U_c coming from (38).

(iii) (53a) and (53b) express the non-penetrability condition for the walls S^+ and S^-. The scalar product $U \cdot n$ is extracted from (45) with $n = 0$ and with $U_c \cdot n$ coming from (38).

(iv) (54) is the expression of (40) in terms of the vector components, and ensures the continuity of the velocity field in the core.

(v) (55) is the expression of (39) in terms of the vector components, and ensures the continuity of the electric current field in the core.

$$-J_{2Y}Z'_2 + J_{2Z} - \frac{Gr}{Ha^2}Z'_2 Z_2 - \frac{Ha^{-2}}{2}[M^+_{0t}(1+Z'^2_2)^{\frac{1}{2}}]' = 0, \tag{51a}$$

$$J_{2Y}Z'_1 - J_{2Z} + \frac{Gr}{Ha^2}Z'_1 Z_1 - \frac{Ha^{-2}}{2}[M^-_{0t}(1+Z'^2_1)^{\frac{1}{2}}]' = 0, \tag{51b}$$

$$U_{2X} + Z_2 J'_{2Z} - \frac{Gr}{Ha^2}Z_2 + \frac{M^+_{0t}(1+Z'^2_2)^{\frac{1}{2}}}{2Ha} = 0, \tag{52a}$$

$$-U_{2Y} - Z'_2 U_{2Z} + Z'_2 Z_2 J'_{2X} - \frac{M^+_{0X}(1+Z'^2_2)}{2Ha} = 0, \tag{52b}$$

$$U_{2X} + Z_1 J'_{2Z} - \frac{Gr}{Ha^2}Z_1 + \frac{M^-_{0t}(1+Z'^2_1)^{\frac{1}{2}}}{2Ha} = 0, \tag{52c}$$

$$U_{2Y} + Z'_1 U_{2Z} - Z'_1 Z_1 J'_{2X} - \frac{M^-_{0X}(1+Z'^2_1)}{2Ha} = 0, \tag{52d}$$

$$-Z'_2 U_{2Y} + U_{2Z} - Z_2 J'_{2Y} + \frac{Ha^{-2}}{2}[M^+_{0X}(1+Z'^2_2)]' = 0, \tag{53a}$$

$$Z'_1 U_{2Y} - U_{2Z} + Z_1 J'_{2Y} - \frac{Ha^{-2}}{2}[M^-_{0X}(1+Z'^2_1)]' = 0, \tag{53b}$$

$$U'_{2Y} = J'_{2X}, \tag{54}$$

$$J'_{2Y} = 0. \tag{55}$$

For this fully established flow, the boundary conditions for these equations are simply the conditions of zero mass and electric current fluxes in the X- and Y-directions. These yield the following scalar conditions:

$$\int_{Y_{\min}}^{Y_{\max}} \int_{Z_2}^{Z_1} \boldsymbol{J} \cdot \boldsymbol{e}_X \, \mathrm{d}Z \, \mathrm{d}Y = 0, \tag{56}$$

$$\forall Y \in [Y_{\min}; Y_{\max}], \quad \int_{Z_2}^{Z_1} \boldsymbol{J} \cdot \boldsymbol{e}_Y \, \mathrm{d}Z = 0, \tag{57}$$

$$\int_{Y_{\min}}^{Y_{\max}} \int_{Z_2}^{Z_1} \boldsymbol{U} \cdot \boldsymbol{e}_X \, \mathrm{d}Z \, \mathrm{d}Y = 0, \tag{58}$$

$$\forall Y \in [Y_{\min}; Y_{\max}], \quad \int_{Z_2}^{Z_1} \boldsymbol{U} \cdot \boldsymbol{e}_Y \, \mathrm{d}Z = 0. \tag{59}$$

The conditions (56) and (58) mean that the ends of the cavity are closed with insulating impermeable walls. The conditions (57) and (59) express the facts that there are no line sources or sinks of mass or electric current along the cylinder walls and that any part of the cylinder walls which is parallel to the magnetic field is electrically insulating and impermeable.

Let us now solve this system of equations. First, the subsystem (52 b), (52 d), (53 a), (53 b), (54), (55) with conditions (56), (59), yields the partial solution:

$$M_{0X}^+ = M_{0X}^- = U_{2Y} = U_{2Z} = J_{2X} = 0. \qquad (60)$$

Secondly, substituting $M_{0t}^+(1+Z_2'^2)^{\frac{1}{2}}$ and $M_{0t}^-(1+Z_1'^2)^{\frac{1}{2}}$ in (51 a), (51 b) with the help of (52 a) and (52 c), and considering the sum and the difference of the two equations obtained, we get

$$Z_1'\left[J_{2Y}+\frac{Gr}{Ha^2}Z_1\right]-Z_2'\left[J_{2Y}+\frac{Gr}{Ha^2}Z_2\right]$$

$$+Ha^{-1}\left[2U_{2X}'+((Z_1+Z_2)J_{2Z}')'-\frac{Gr}{Ha^2}(Z_1+Z_2)'\right]=0, \quad (61)$$

$$2J_{2Z}+Z_1'\left[-J_{2Y}-\frac{Gr}{Ha^2}Z_1\right]+Z_2'\left[-J_{2Y}+\frac{Gr}{Ha^2}Z_2\right]$$

$$+Ha^{-1}\left[((Z_2-Z_1)J_{2Z}')'+\frac{Gr}{Ha^2}(Z_1-Z_2)'\right]=0. \quad (62)$$

The above equations and (52 a), (52 c), (55) allow us to find expressions for $J_{2Y}, J_{2Z}, U_{2X}, M_{0t}^+, M_{0t}^-$. Conditions (57) and (58) now become:

$$\forall Y \in [Y_{\min}; Y_{\max}],$$

$$J_{2Y}(Z_1-Z_2)+\frac{Gr}{2Ha^2}(Z_1^2-Z_2^2)-\frac{M_{0t}^+(1+Z_2'^2)^{\frac{1}{2}}}{2Ha^2}-\frac{M_{0t}^-(1+Z_1'^2)^{\frac{1}{2}}}{2Ha^2}=0, \quad (63)$$

$$\int_{Y_{\min}}^{Y_{\max}}\left[U_{2X}(Z_1-Z_2)+\frac{J_{2Z}'-Gr\,Ha^{-2}}{2}(Z_1^2-Z_2^2)\right.$$

$$\left.+\frac{M_{0t}^+(1+Z_2'^2)}{2Ha^2}+\frac{M_{0t}^-(1+Z_1'^2)}{2Ha^2}\right]dY=0. \quad (64)$$

Substituting $M_{0t}^+(1+Z_2'^2)^{\frac{1}{2}}$ and $M_{0t}^-(1+Z_1'^2)^{\frac{1}{2}}$ in (63) and using once more (52 a) and (52 c) yield

$$Z_1\left[J_{2Y}+\frac{Gr}{2Ha^2}Z_1\right]-Z_2\left[J_{2Y}+\frac{Gr}{2Ha^2}Z_2\right]$$

$$+Ha^{-1}\left[2U_{2X}+((Z_1+Z_2)J_{2Z}')-\frac{Gr}{Ha^2}(Z_1+Z_2)\right]=0. \quad (65)$$

Equation (65) is an integral of (61). We hence must solve (65), (62), (52 a), (52 c) and (55) with condition (64). We limit ourselves to an approximate method (of order Ha^{-1}), which is not penalizing since the precision obtained in the general method of the §2 is also of order Ha^{-1}. Let us suppose that J_{2Z} is not large compared to Gr/Ha^2 (we shall check this hypothesis later). So, (62) yields (with an approximation error of order Ha^{-1})

$$J_{2Z}=\frac{Gr}{Ha^2}\left(\frac{Z_1^2+Z_2^2}{4}\right)'+J_{2Y}\left(\frac{Z_1+Z_2}{2}\right)', \qquad (66)$$

and (65) can be rewritten (if U_{2X} is very large compared to Gr/Ha^2)

$$U_{2X}=-\frac{Gr}{Ha}\left(\frac{Z_1^2-Z_2^2}{4}\right)-Ha\,J_{2Y}\left(\frac{Z_1-Z_2}{2}\right). \qquad (67)$$
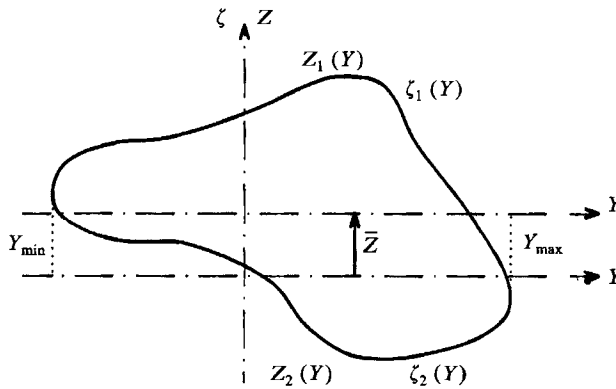
FIGURE 2. The change of frame of reference.

Let us now take into account condition (64), written as follows:

$$\int_{Y_{\min}}^{Y_{\max}} \frac{Gr}{Ha^2}\left[\left(\frac{Z_1^2+Z_2^2}{4}\right)'' - 1\right]\left(\frac{Z_1^2-Z_2^2}{2}\right)\mathrm{d}Y - \int_{Y_{\min}}^{Y_{\max}} \frac{Gr}{Ha}\left(\frac{Z_1^2-Z_2^2}{4}\right)(Z_1-Z_2)\,\mathrm{d}Y$$

$$+ J_{2Y}\int_{Y_{\min}}^{Y_{\max}}\left(\frac{Z_1+Z_2}{2}\right)''\left(\frac{Z_1^2-Z_2^2}{2}\right)\mathrm{d}Y - J_{2Y}\int_{Y_{\min}}^{Y_{\max}}\frac{Ha(Z_1-Z_2)^2}{2}\mathrm{d}Y$$

$$+ \int_{Y_{\min}}^{Y_{\max}}\frac{M_{0t}^+(1+Z_2'^2)+M_{0t}^-(1+Z_1'^2)}{2Ha^2}\mathrm{d}Y = 0. \quad (68)$$

Equations (52a) and (52c) indicate that

$$\frac{M_{0t}^+}{Ha^2} = O\left(\frac{Gr}{Ha^2}\right)+O(J_{2Y}) \quad \text{and} \quad \frac{M_{0t}^-}{Ha^2} = O\left(\frac{Gr}{Ha^2}\right)+O(J_{2Y}). \quad (69)$$

It is thus correct to neglect the first, the third and the fifth terms of (68) compared to the other terms since the precision of our analysis is of order Ha^{-1}. We then obtain

$$J_{2Y} = -\frac{Gr}{Ha^2}\frac{\displaystyle\int_{Y_{\min}}^{Y_{\max}}\left(\frac{Z_1^2-Z_2^2}{2}\right)(Z_1-Z_2)\,\mathrm{d}Y}{\displaystyle\int_{Y_{\min}}^{Y_{\max}}(Z_1-Z_2)^2\,\mathrm{d}Y} = O\left(\frac{Gr}{Ha^2}\right). \quad (70)$$

Let us now return to the hypotheses we made. The value of J_{2Z} is actually of order Gr/Ha^2 and U_{2X} is large compared to Gr/Ha^2 (it is of order Gr/Ha); our assumptions are justified except in a particular case, i.e. when $Z_2+Z_1 = 0$. Nevertheless, in this case, (65) leads to $U_{2X} = 0$ and (67) leads to the same result when substituting J_{2Y} with the help of (70). This means that (66) and (67) together with the (70) are valid in any case.

The solution is now completed. A change of coordinates in the cross-sectional plane leads to simplifications in the formula for the results. A new frame of reference (Y, ζ) is obtained by a translation of magnitude $\bar{Z}$ of the former (Y, Z) frame in the Z-direction (see figure 2):

$$\bar{Z} = \int_{Y_{\min}}^{Y_{\max}}\left(\frac{Z_1+Z_2}{2}\right)(Z_1-Z_2)^2\,\mathrm{d}Y \bigg/ \int_{Y_{\min}}^{Y_{\max}}(Z_1-Z_2)^2\,\mathrm{d}Y. \quad (71)$$

(a)

$$\zeta_1 = (\tfrac{1}{4} - Y^2)^{\frac{1}{2}}, \quad \zeta_2 = -\zeta_1$$

$$\boldsymbol{U}_c = -2\frac{Gr}{Ha^2}\zeta\boldsymbol{e}_X$$

$$\boldsymbol{J}_c = \frac{Gr}{Ha^2}\zeta\boldsymbol{e}_Y - \frac{Gr}{Ha^2}Y\boldsymbol{e}_Z$$

$$\Phi_c = \frac{Gr}{Ha^2}Y\zeta$$

(b)

$$\zeta_1 = \tfrac{1}{2}, \quad \zeta_2 = -\tfrac{1}{2},$$

$$\boldsymbol{U}_c = -\frac{Gr}{Ha^2}\zeta\boldsymbol{e}_X$$

$$\boldsymbol{J}_c = \frac{Gr}{Ha^2}\zeta\boldsymbol{e}_Y$$

$$\Phi_c = c^{ste}$$

(c)

$$\zeta_1 = Y + \tfrac{1}{2}, \quad \zeta_2 = -Y - \tfrac{1}{2} \quad \text{if } Y < 0$$

$$\boldsymbol{U}_c = \boldsymbol{0}$$

$$\boldsymbol{J}_c = \frac{Gr}{Ha^2}\zeta\boldsymbol{e}_Y + \frac{Gr}{Ha^2}(Y + \tfrac{1}{2})\boldsymbol{e}_Z$$

$$\Phi_c = -\frac{Gr}{Ha^2}(Y + \tfrac{1}{2})\zeta$$

$$\zeta_1 = -Y + \tfrac{1}{2}, \quad \zeta_2 = Y - \tfrac{1}{2} \quad \text{if } Y > 0$$

$$\boldsymbol{U}_c = \boldsymbol{0}$$

$$\boldsymbol{J}_c = \frac{Gr}{Ha^2}\zeta\boldsymbol{e}_Y + \frac{Gr}{Ha^2}(Y - \tfrac{1}{2})\boldsymbol{e}_Z$$

$$\Phi_c = -\frac{Gr}{Ha^2}(Y - \tfrac{1}{2})\zeta$$
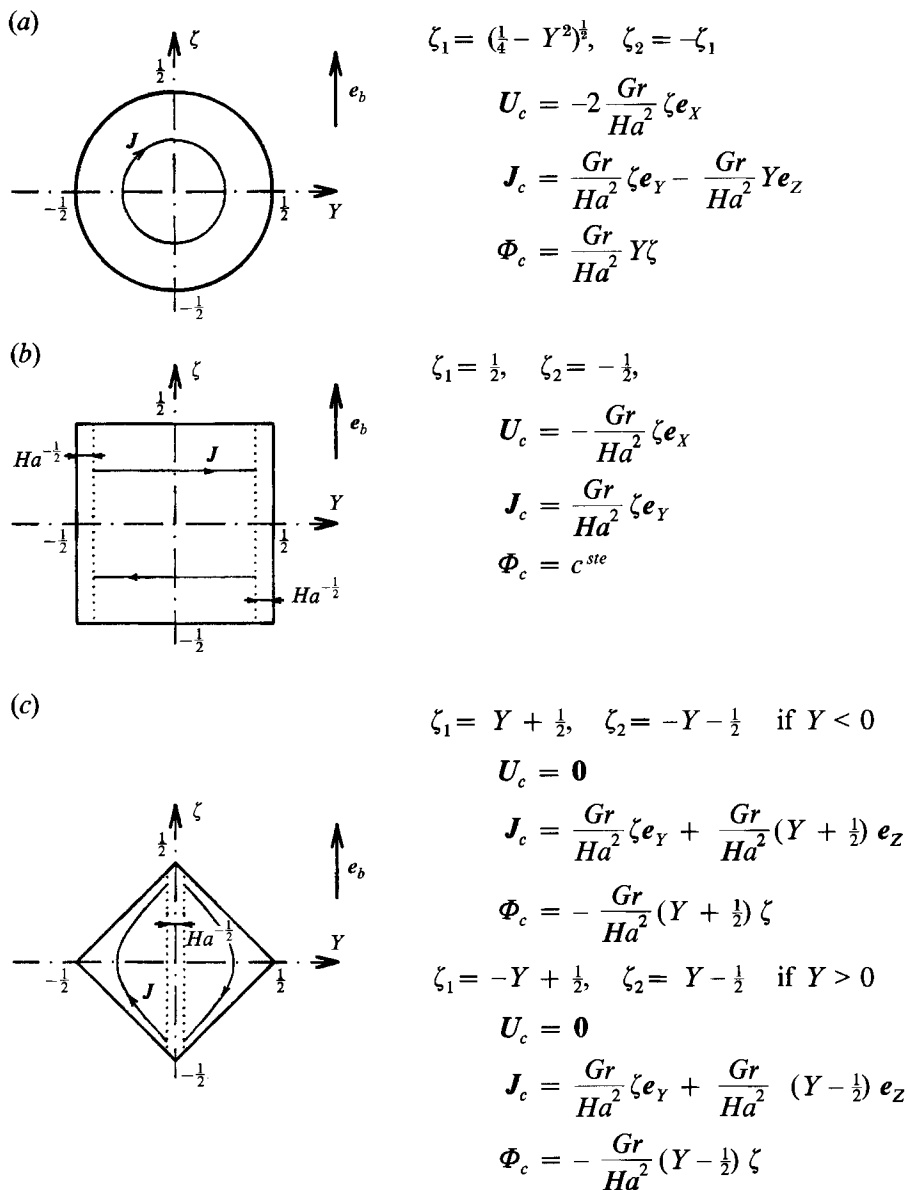
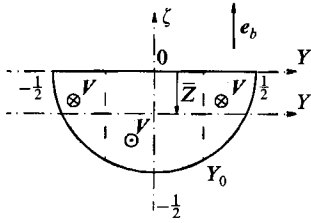FIGURE 3(*a–c*). For caption see facing page.

In the new frame of reference (Y, ζ), the contour functions ζ_1 and ζ_2 take the forms $\zeta_1 = Z_1 - \bar{Z}$ and $\zeta_2 = Z_2 - \bar{Z}$. The core solution in this new frame is

$$\boldsymbol{U}_c = \left\{\frac{Gr}{Ha^2}\left[\left(\frac{\zeta_1^2 + \zeta_2^2}{4}\right)'' - 1\right]\zeta - \frac{Gr}{Ha}\left(\frac{\zeta_1^2 - \zeta_2^2}{4}\right)\right\}\boldsymbol{e}_X, \tag{72}$$

$$\boldsymbol{J}_c = \frac{Gr}{Ha^2}\zeta\boldsymbol{e}_Y + \frac{Gr}{Ha^2}\left(\frac{\zeta_1^2 + \zeta_2^2}{4}\right)'\boldsymbol{e}_Z, \tag{73}$$

$$\Phi_c = -\frac{Gr}{Ha^2}\left(\frac{\zeta_1^2 + \zeta_2^2}{4}\right)'\zeta + \frac{Gr}{Ha}\int_{Y_{min}}^{Y}\left(\frac{\zeta_1^2 - \zeta_2^2}{4}\right)dY. \tag{74}$$

(*d*)

$$\bar{Z} = -\frac{3^2\pi}{2^7} \approx -0.2209, \quad \zeta_1 = \frac{3^2\pi}{2^7}, \quad \zeta_2 = -(\tfrac{1}{4}-Y^2)^{\frac{1}{2}} + \frac{3^2\pi}{2^7}$$

$$U_c = \left\{\frac{Gr}{Ha^2}\left[\frac{3^2\pi}{2^8}\left[(\tfrac{1}{4}-Y^2)^{-\frac{1}{2}} + Y^2(\tfrac{1}{4}-Y^2)^{-\frac{3}{2}}\right] - \frac{3}{2}\right]\zeta \right.$$

$$\left. + \frac{Gr}{Ha}\left[\frac{(\tfrac{1}{4}-Y^2)}{4} - \frac{3^2\pi}{2^8}(\tfrac{1}{4}-Y^2)^{\frac{1}{2}}\right]\right\}e_X$$

$$J_c = \frac{Gr}{Ha^2}\zeta e_Y + \frac{Gr}{Ha^2}\left[\frac{3^2\pi}{2^8}Y(\tfrac{1}{4}-Y^2)^{\frac{1}{2}} - \frac{Y}{2}\right]e_Z$$

$$\Phi_c = -\frac{Gr}{Ha^2}\left[\frac{3^2\pi}{2^8}Y(\tfrac{1}{4}-Y^2)^{\frac{1}{2}} - \frac{Y}{2}\right]\zeta$$

$$+ \frac{Gr}{Ha}\left[\frac{Y^3}{12} + \frac{1}{92} + \frac{3^2\pi}{2^9}\left((\pi + \alpha) - \frac{\sin 2\alpha}{2}\right)\right]$$

where α is such that: $\sin\alpha = 2Y$ and $\alpha \in [-\pi ; 0]$. The values of Y where the velocity changes its sign are $\pm Y_0 = \left(\frac{1}{4} - \frac{3^4\pi}{2^{12}}\right)^{\frac{1}{2}}$.

(*e*)

$$\bar{Z} = -\tfrac{3}{16} \approx -0.1875, \quad \zeta_1 = \tfrac{3}{16}$$

$$\zeta_2 = -Y - \tfrac{5}{16} \quad \text{if } Y < 0$$

$$U_c = \left[-2\frac{Gr}{Ha^2}\zeta + \frac{Gr}{Ha}\left(\frac{1}{64} + \frac{5}{32}Y + \frac{Y^2}{4}\right)\right]e_X$$

$$J_c = \frac{Gr}{Ha^2}\zeta e_Y + \frac{Gr}{Ha^2}\left(\frac{5}{32} + \frac{Y}{2}\right)e_Z$$

$$\Phi_c = -\frac{Gr}{Ha^2}\left(\frac{5}{32} + \frac{Y}{2}\right)\zeta$$

$$+ \frac{Gr}{Ha}\left(\frac{Y}{64} + \frac{5}{64}Y^2 + \frac{Y^3}{12}\right)$$

$$\zeta_1 = \tfrac{3}{16}, \quad \zeta_2 = Y - \tfrac{5}{16} \quad \text{if } Y > 0$$

$$U_c = \left[-\frac{Gr}{2Ha^2}\zeta + \frac{Gr}{Ha}\left(\frac{1}{64} - \frac{5}{32}Y + \frac{Y^2}{4}\right)\right]e_X$$

$$J_c = \frac{Gr}{Ha^2}\zeta e_Y + \frac{Gr}{Ha^2}\left(-\frac{5}{32} + \frac{Y}{2}\right)e_Z$$

$$\Phi_c = -\frac{Gr}{Ha^2}\left(-\frac{5}{32} + \frac{Y}{2}\right)\zeta$$

$$- \frac{Gr}{Ha}\left(\frac{Y}{64} - \frac{5}{64}Y^2 + \frac{Y^3}{12}\right)$$

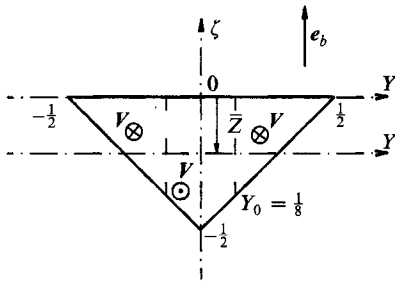FIGURE 3. Results obtained for various cross-sectional shapes.

The expression for Φ_c comes from the integration of Ohm's law (11) with the help of the above expressions for U_c and J_c. The solution in the Hartmann layers is now straightward from equations ($52a$) and ($52c$); for the velocity field, we already know that it reaches a value of zero at the walls in an exponentially decreasing manner.

3.2.2. *Some cross-sectional shapes*

The functions ζ_1 and ζ_2 have a great influence on the melt motion. On the one hand, in the case of a symmetric cross-section ($Z_1 + Z_2 = $ constant, or equivalently $\zeta_2 = -\zeta_1$ according to the formula (71)), the velocity field is of order Gr/Ha^2 (instead of Gr/Ha), and on the other hand, these functions intervene also through their first and second derivatives. Figure 3 presents the results obtained for some cross-section shapes. Some characteristic features are noticeable:

(i) There are parallel layers for a square cross-section (on both sides $Y = \pm\frac{1}{2}$), a 45° inclined square cross-section (along the line $Y = 0$), and a triangular one (along the line $Y = 0$). These layers accommodate jumps in electric current and electric potential between two cores or between the core and a wall. Our present study does not include the solution there.

(ii) For the semicircular cross-section, we notice a singularity at the corners $Y = \pm\frac{1}{2}$. Nevertheless each singularity involves a finite mass flow of order Gr/Ha^2, so that our solution is correct in the high Hartmann number limit and is well-represented by the Gr/Ha part. The velocity field varies mainly in the Y-direction; it is positive in the centre of the cavity and negative on the sides.

3.3. *Perfectly electrically conducting walls*

The only change from the insulating case is the electrical condition at the walls: $J \wedge n = 0$, instead of $J \cdot n = 0$. In the system (51)–(55), the equation ($51a$) (resp. ($51b$)) is replaced by ($75a$) and ($75b$) (resp. ($75c$) and ($75d$)) below that express the condition of zero tangential part of the electric current along e_X and t at the wall S^+ (resp. at the wall S^-). The tangential part of J is given by (41) where $n = 0$ and where J_c results from (37),

$$J_{2X} + M_{0X}^+/2Ha = 0, \tag{75a}$$

$$-J_{2Y} - Z_2' J_{2Z} + \frac{M_{0t}^+(1 + Z_2'^2)^{\frac{1}{2}}}{2Ha} - \frac{Gr}{Ha^2} Z_2 = 0, \tag{75b}$$

$$J_{2X} - M_{0X}^-/2Ha = 0, \tag{75c}$$

$$J_{2Y} + Z_1' J_{2Z} - \frac{M_{0t}^-(1 + Z_1'^2)^{\frac{1}{2}}}{2Ha} + \frac{Gr}{Ha} Z_1 = 0. \tag{75d}$$

Among the boundary conditions (56)–(59) considered, only (58) and (59) still hold. The others dealt with electric charge conservation in the fluid, but now electric current can freely circulate in the walls. Nevertheless, we must specify the way our two surfaces S^+ and S^- are electrically connected. We here assume that they are in contact, so their electric potentials are the same.

Equations ($75a, c$), ($52b, d$), ($53a, b$), (54) and (55) considered with the condition (59) lead to

$$M_{0X}^+ = M_{0X}^- = U_{2Y} = U_{2Z} = J_{2X} = 0. \tag{76}$$

We now must solve ($75b, d$), ($52a, c$) and (55) with the help of (58), and with the equality of the potentials of the two walls. As for the insulating case, substituting

$M_{0t}^{+}(1+Z_2'^2)^{\frac{1}{2}}$ and $M_{0t}^{-}(1+Z_1'^2)^{\frac{1}{2}}$ in $(75b, d)$ with the help of $(52a, c)$ and taking the sum and the difference of the equations obtained, gives

$$U_{2X} + (Z_2 J_{2Z})' + J_{2Y} = 0, \tag{77a}$$

$$U_{2X} + (Z_1 J_{2Z})' + J_{2Y} = 0. \tag{77b}$$

These last equations imply that $J_{2Z} = \text{constant}/(Z_1 - Z_2)$. Let us now write that S^+ and S^- have the same electric potential:

$$\Phi_{s^+} = \Phi_{s^-}. \tag{78}$$

Since Ohm's law (11) gives $\partial\Phi/\partial Z = -J_{2Z}$, integrating between the two walls leads to $J_{2Z}(Z_1 - Z_2) = 0$. So the result is

$$J_{2Z} = 0. \tag{79}$$

Using $(52a)$ and $(52c)$, condition (58) becomes

$$\int_{Y_{\min}}^{Y_{\max}} \left\{ -(Z_1 - Z_2)J_{2Y} - \frac{Gr}{Ha^2}\left(\frac{Z_1^2 - Z_2^2}{2}\right) \right.$$
$$\left. + \frac{(1+Z_2'^2)^{\frac{1}{2}}}{Ha}\left(J_{2Y} + \frac{Gr}{Ha^2}Z_2\right) + \frac{(1+Z_1'^2)^{\frac{1}{2}}}{Ha}\left(J_{2Y} + \frac{Gr}{Ha^2}Z_1\right) \right\} dY = 0. \tag{80}$$

At the order Ha^{-1}, the solution of J_{2Y} is

$$J_{2Y} = -\frac{Gr}{Ha^2} \int_{Y_{\min}}^{Y_{\max}}\left(\frac{Z_1 + Z_2}{2}\right)(Z_1 - Z_2)\,dY \Bigg/ \int_{Y_{\min}}^{Y_{\max}}(Z_1 - Z_2)\,dY, \tag{81}$$

and $(77a)$ and $(77b)$ give

$$U_{2X} = \frac{Gr}{Ha^2} \int_{Y_{\min}}^{Y_{\max}}\left(\frac{Z_1 + Z_2}{2}\right)(Z_1 - Z_2)\,dY \Bigg/ \int_{Y_{\min}}^{Y_{\max}}(Z_1 - Z_2)\,dY. \tag{82}$$

Let us again change our coordinate system in order to make the expression for the solution more tractable. The variable $\bar{Z}$ is here

$$\bar{Z} = \int_{Y_{\min}}^{Y_{\max}}\left(\frac{Z_1 + Z_2}{2}\right)(Z_1 - Z_2)\,dY \Bigg/ \int_{Y_{\min}}^{Y_{\max}}(Z_1 - Z_2)\,dY. \tag{83}$$

Considering the new frame of reference (Y, ζ) resulting of the translation of magnitude $\bar{Z}$ in the Z-direction, the solution for the core becomes

$$U_c = -\frac{Gr}{Ha^2}\zeta e_X, \tag{84}$$

$$J_c = \frac{Gr}{Ha^2}\zeta e_Y, \tag{85}$$

$$\Phi_c = \text{constant}, \tag{86}$$

where the electric potential is given by Ohm's law (11). An important feature is the fact that the solution does not depend on the cross-section shape, except through the calculation of $\bar{Z}$ which indicates the position of the new origin. Notice that in the case of a symmetric cross-section, the new frame of reference still coincides with the symmetry axis (formula (83)). Concerning non-symmetric cross-sections, we find now that for the semicircle and triangle respectively, $\bar{Z}$ has the value

$$\bar{Z} = -\frac{2}{3\pi} \approx -0.2122, \quad \bar{Z} = -\tfrac{1}{6} \approx -0.1667. \tag{87}$$

The key result is that for any cross-section shape the velocity field is of order Gr/Ha^2 (equation (84)) as opposed to the case of electrically insulating walls.

Remark Ohm's law (11) and the zero velocity condition at the walls show that any electric current entering the walls is caused by a potential gradient in the Hartmann layer. However, we here observe that an electric current crosses the Hartmann layer (85) and that the electric potential is uniform, (86). This paradox can be solved if we keep in mind the order of precision of our solution (Ha^{-1} for U and J): thus the potential is uniform with non-uniformities of order $Gr\,Ha^{-3}$. A change of this magnitude across the characteristic thickness of the Hartmann layer ($\delta = O(Ha^{-1})$) is enough for the current (85) to circulate. Such an Ha^{-1} variation of the electric potential through the Hartmann layer also arises in pressure-driven duct flows.

4. Concluding remarks

The relevant variables in this work are U and J; we did not consider the induced magnetic field (often called b). This variable b is generally of interest in duct flows (in Elsasser's variables for instance), although it is assumed to be very small compared to the imposed uniform magnetic field B ($R_m \ll 1$). This variable can be useful when its boundary conditions are explicit as is the case for fully established parallel flows: b is zero outside the electrically conducting domain. Except in these configurations, it would be false to assume any arbitrary boundary condition (we only know that b tends towards zero far enough from the conducting domain). For the variables U and J, explicit boundary conditions are generally known, which is why they have been chosen.

A special emphasis was given to the variables M^+ and M^- defined in §2. They are useful not only as a tool for solving the problem but they also clearly show the structure of the flow: the core flow (21), (22) or the boundary layer flow (25), (26). The method employed is general and can be applied to a large class of flows: one can change the geometry, the boundary conditions (free surfaces, Seebeck effect,...), or the driving force. It is always possible to extract the corresponding two-dimensional equations for the three-dimensional problem (see §2), but in the general case, we have not presented the boundary conditions for these two-dimensional equations. When this is done (which implies studying the parallel layer), it will be possible to affirm that the dimension of the problem was indeed reduced.

The most striking result in §3 concerns the case of electrically insulating walls. For non-symmetric cross-sections, the velocity field is of order Gr/Ha, whereas it is of order Gr/Ha^2 in the symmetric case. It is interesting to notice that the part of the solution due to the asymmetry is more difficult to obtain. If we had only considered symmetric cross-sectional shapes, it would not have been necessary to find (42) and (45) at the walls S^+ and S^-. Global conservations and simple relations in the Hartmann layers (tangential parts (41) and (44)) would have been enough to get the solution. For instance, Chang & Lundgren (1961) give the solution for a pressure-driven flow in symmetric ducts with thin walls of arbitrary electric conductance without calculating the normal component of the electric current near the walls. Their method could not have been extended to the case of non-symmetric cross-sections. We can say that (42) and (45) enable us to quantify the electrical exchanges between a Hartmann layer and the neighbouring core. In this case of electrically insulating walls, it is useful to have in mind a heuristic understanding of the fundamental difference between symmetrical and asymmetrical results. The momentum equation in the core, $Ha^2(e_b \cdot \nabla)\,J = Gr\,e_Y$, and the continuity equation, $\nabla \cdot J = 0$, imply after some elementary operations that J_Y does not depend on Y and that its derivative along Z is $Gr\,Ha^{-2}$. For symmetrical cross-

sections, J_Y is zero at the symmetry axis, and the electric current Y-flux in the core is zero for any value of Y. The electric potential gradient is not very large compared to J_Y so that Ohm's law implies that U scales as $Gr\,Ha^{-2}$. For asymmetrical cross-sections, for some values of Y, the Y-component of the electric current flux must obviously be of order $Gr\,Ha^{-2}$ in the core. An opposite electric current flux must flow in the Hartmann layers. Then a classical result of MHD, expressed in our analysis as 'M^+ or M^- has no Hartmann layer for a given side', states that U scales as $Gr\,Ha^{-1}$.

Let us now examine whether our analysis really applies for crystal growth experiments. A key point is the non-inertia assumption (see §2, hypothesis iii) which is closely related to the fully established hypothesis of §3. There is experimental and numerical evidence that at low Grashof number, with no magnetic field, the flow is fully established (Bontoux *et al.* 1986) excepted in recirculating end regions. Moreover, Gershuni & Zhukhovitskii (1972) have shown for a two-dimensional flow that a magnetic field increases the critical Grashof number above which the inertialess fully established flow is no longer stable. Using our solutions, it is possible to estimate the interaction parameter $N = Ha^2\,Re^{-1}$. The Reynolds number Re is $Gr\,Ha^{-2}$ except for insulating walls and asymmetric cross-sections for which it is $Gr\,Ha^{-1}$, hence N scales as $Ha^4\,Gr^{-1}$ or $Ha^3\,Gr^{-1}$. Considering typical values for Gr about 10^5–10^6 and for Ha about 10^2–10^3, N is higher than unity.

To conclude, our results show that for the horizontal Bridgman process with a magnetic field, changing the crucible geometry does change the velocity distribution in the case of insulating crucibles. For instance, the velocity may be zero in some regions for instance with a 45° inclined square cross-section (see figure 3). Moreover, this paper gives interesting velocity orders of magnitude. It is important to notice the dramatic sensitivity of the velocity to the exact geometry when the walls are insulating: a symmetry defect entails an Ha-amplified modification of the velocity. This gives a magnetic sense to the symmetry concept: geometric defects must be of order less than the Hartmann-layer characteristic thickness ($\delta = O(Ha^{-1})$). When symmetry arguments are used *a priori* (axisymmetry, plane symmetry ...), they may be in fact a very rough approximation and perhaps a mistake. Of course, apart from geometric aspects, one can wonder about the required accuracy of the other parameters such as the thermal gradient or the magnetic field itself.

Appendix

We obtain here the results for the Hartmann layers ((33)–(36)). We must solve the equations (25), (26) and (27), (28) when $\cos\theta$ is not zero.

A.1. *First expression*

Let us consider (31) and (32) which are an approximate form of (25) and (26). Notice that on the surface $S^-(\cos\theta < 0)$ a solution of (31) is either zero or exponentially growing in the fluid direction. This last result is physically unacceptable, so we can conclude that the variable M^+ does not have a boundary layer on the surface S^-. In the same manner, M^- has no boundary layer at S^-. On the contrary, (31) on the surface S^+ ($\cos\theta > 0$), and (32) on the S^- surface take the same form

$$Ha|\cos\theta|\frac{\partial(M-M_c)}{\partial n}[1+O(Ha^{-1})]+\frac{\partial^2(M-M_c)}{\partial n^2}[1+O(Ha^{-2})] = 0, \qquad \text{(A 1)}$$

leading to decreasing exponential solutions

$$M - M_c = A \, \mathrm{e}^{-Ha|\cos\theta|n}, \qquad (A\,2)$$

where A does not depend on the n-coordinate.

A.2. *Expected accuracy for dynamics*

Let us return to the initial equations (25) and (26) and estimate the difference between their actual solutions and (A 2). Let us first rewrite (25) and (26) distinguishing the derivative terms along n:

$$Ha|\cos\theta|\frac{\partial[M-M_c]}{\partial n} \pm Ha\sin\theta(t\cdot\nabla)[M-M_c] + \frac{\partial^2[M-M_c]}{\partial n^2} + \Delta_t[M-M_c] = 0, \quad (A\,3)$$

where t is a tangent to the surface in the plane of e_b and n, and Δ_t denotes the Laplacian operator in the tangent space to the surface. *A posteriori*, we can estimate the orders of magnitude of the second and fourth terms in (A 3) which were neglected to get (A 2):

$$Ha(t\cdot\nabla)[M-M_c] = (Ha\,O(A) + Ha^2\,O(An))\,\mathrm{e}^{-Ha|\cos\theta|n}, \qquad (A\,4)$$

$$\Delta_t[M-M_c] = (O(A) + Ha\,O(An) + Ha^2\,O(An^2))\,\mathrm{e}^{-Ha|\cos\theta|n}, \qquad (A\,5)$$

since $(t\cdot\nabla)A = O(A)$ and $(t\cdot\nabla)\mathrm{e}^{-Ha|\cos\theta|n} = O(n\,Ha\,\mathrm{e}^{-Ha|\cos\theta|n})$. In order to take these terms into account, we need only include the following uncertainty on the form of the solutions:

$$M - M_c = A\,\mathrm{e}^{-Ha|\cos\theta|n} + O(An\,\mathrm{e}^{-Ha|\cos\theta|n}). \qquad (A\,6)$$

The added term leads to corrections in (25) and (26) which are of the form (A 4) and (A 5). Thus (A 6) corresponds to the general solution of (25) and (26). The solutions of form (A 2) are correct at the Ha^{-1} order with respect to (25) and (26).

A.3. *About continuity*

Let us now examine what is implied by the continuity equations (27) and (28). In a general form, they are

$$\nabla\cdot(M-M_c) = 0. \qquad (A\,7)$$

The divergence of (A 2) is

$$(\nabla\cdot A - Ha|\cos\theta|A\cdot n - Ha\,nA\cdot\nabla|\cos\theta|)\,\mathrm{e}^{-Ha|\cos\theta|n} = 0. \qquad (A\,8)$$

We have applied the vector analysis formula: $\nabla\cdot ab = a\nabla\cdot b + b\cdot\nabla a$, and, if the scalar function is $a = \mathrm{e}^{-Ha|\cos\theta|n}$, then we have: $\nabla a = (-|\cos\theta|n - n\nabla|\cos\theta|)\,Ha\,a$. The normal component of the vector field A must be of order Ha times smaller than the tangential ones. We are led to the following estimate:

$$M - M_c = M_0\,\mathrm{e}^{-Ha|\cos\theta|n}, \qquad (A\,9)$$

where M_0 does not depend on the n-coordinate and is strictly tangent to the surface. However we notice that (A 9) can never fulfil (A 7) at the Ha^{-1} order when $\cos\theta$ changes: the term with the linear variation with n in (A 8) is of the same order of magnitude as M_0. We must add a term whose divergence could compensate for this linear term. In order to satisfy (A 7), the solution (A 6) must have the form

$$M - M_c = \left[M_0 + \frac{n}{Ha}\nabla_s\cdot\left(\frac{M_0}{|\cos\theta|}\right) - n\frac{M_0\cdot\nabla|\cos\theta|}{|\cos\theta|}n + E_n + E_t\right]\mathrm{e}^{-Ha|\cos\theta|n}, \quad (A\,10)$$

where $E_t = O(M_0 n)$ is tangent to S, and $E_n = O(M_0 n/Ha)$ is normal to S. Since the function $n\,\mathrm{e}^{-Han}$ is not greater than Ha^{-1}, we obtain (33)–(36) from (A 10). One can check that the divergence of (A 10) is of order Ha times smaller than the vector field

given by (A 10) itself. So this expression is a solution of both (A 1) and (A 7) at the order Ha^{-1}.

A.4. *The Hartmann-layer extension*

How far from the wall does (A 10) reflect the actual flow in the Hartmann layer? The answer is: as far as its magnitude is greater than the uncertainty of our solution in the core flow. This criterion typically leads to a distance ϵ such that $e^{-Ha\epsilon} \approx Ha^{-1}$, so that $\epsilon \approx \ln Ha/Ha$.

This distance is not the characteristic thickness of the variations of the solutions in the Hartmann layer, $\delta \approx Ha^{-1}$; indeed, the derivatives of the solutions are of order Ha times greater than the solutions in the Hartmann layer.

REFERENCES

BONTOUX, P., ROUX, B., SCHIROKY, G. H., MARKHAN, B. L. & ROSENBERG, F. 1986 Convection in the vertical midplane of a horizontal cylinder. Comparison of two-dimensional approximations with three-dimensional results. *Intl J. Heat Mass Transfer* **29**, 227–240.

BURTON, J. A., PRIM, R. C. & SLICHTER, W. P. 1953 The distribution of solute in crystals grown from the melt. Part I. Theoretical. *J. Chem. Phys.* **21**, 1987–1996.

CARLSON, D. J. & WITT, A. F. 1992 Quantitative analysis of the effect of vertical magnetic fields on microsegregation on Te-doped LEC GaAs. *J. Cryst. Growth* **116**, 461–472.

CHANDRASEKHAR, S. 1961 *Hydrodynamic and Hydromagnetic Stability.* Dover.

CHANG, C. C. & LUNDGREN, T. S. 1961 Duct flow in magnetohydrodynamics. *Z. Angew. Math. Phys.* **12**, 100–114.

ELSASSER, W. M. 1950 The hydromagnetic equations. *Phys. Rev.* **79**, 183.

GARANDET, J. P., ALBOUSSIÈRE, T. & MOREAU, R. 1992 Buoyancy driven convection in a rectangular enclosure with a transverse magnetic field. *Intl J. Heat Mass Transfer* **35**, 741–748.

GERSHUNI, G. Z. & ZHUKHOVITSKII, E. M. 1972 *Convective Stability of Incompressible Fluids.* Moskva: Izdatel'stvo "Nauka".

HJELLMING, L. N. 1990 A thermal model for Czochralski silicon crystal growth with an axial magnetic field. *J. Cryst. Growth* **104**, 327–344.

HJELLMING, L. N. & WALKER, J. S. 1986 Melt motion in a Czochralski crystal puller with an axial magnetic field: isothermal motion. *J. Fluid Mech.* **164**, 237–273.

HUNT, J. C. R. 1965 Magnetohydrodynamic flow in rectangular ducts. *J. Fluid Mech.* **21**, 577–590.

HUNT, J. C. R. & MALCOLM, D. G. 1968 Some electrically driven flows in magnetohydrodynamics. Part 2. Theory and experiment. *J. Fluid Mech.* **33**, 775–801.

HUNT, J. C. R. & SHERCLIFF, J. A. 1971 Magnetohydrodynamics at high Hartmann number. *Ann. Rev. Fluid Mech.* **3**, 37–62.

HUNT, J. C. R. & STEWARTSON, K. 1965 Magnetohydrodynamic flow in rectangular ducts. Part 2. *J. Fluid Mech.* **23**, 563–581.

KULIKOVSKII, A. G. 1968 Slow steady flows of a conducting fluid at high Hartmann numbers. *Isz. Akad. Nauk. SSSR Mekh. Zhidk. i Gaza* **3**, 3–10.

LANGLOIS, W. E. 1985 Buoyancy-driven flows in crystal-growth melts. *Ann. Rev. Fluid Mech.* **17**, 191–215.

MATTHIESEN, D. H., WARGO, M. J., MOTAKEF, S., CARLSON, D. J., NAKOS, J. S. & WITT, A. F. 1987 Dopant segregation during vertical Bridgman–Stockbarger growth with melt stabilization by strong axial magnetic fields. *J. Cryst. Growth* **85**, 557–560.

MOREAU, R. 1990 *Magnetohydrodynamics.* Kluwer.

MOTAKEF, S. 1990 Magnetic field elimination of convective interference with segregation during vertical-Bridgman growth of doped semiconductors. *J. Cryst. Growth* **104**, 833–850.

SHERCLIFF, J. A. 1953 Steady motion of conducting fluids in pipes under transverse magnetic fields. *Proc. Camb. Phil. Soc.* **49**, 136–144.

SHERCLIFF, J. A. 1956 The flow of conducting fluids in circular pipes under transverse magnetic fields. *J. Fluid Mech.* **1**, 644–666.